PCCP

PAPER

View Article Online
View Journal | View Issue

Cite this: *Phys. Chem. Chem. Phys.*, 2017, **19**, 31581

Counterion effects on the ultrafast dynamics of charge-transfer-to-solvent electrons

N. Rivas,†[a] G. Moriena,[b] L. Domenianni,[a] J. H. Hodak[a] and E. Marceca*[a]

We performed femtosecond transient absorption (TA) experiments to monitor the solvation dynamics of charge-transfer-to-solvent (CTTS) electrons originating from UV photoexcitation of ammoniated iodide in close proximity to the counterions. Solutions of KI were prepared in liquid ammonia and TA experiments were carried out at different temperatures and densities, along the liquid–gas coexistence curve of the fluid. The results complement previous femtosecond TA work by P. Vöhringer's group in neat ammonia *via* multiphoton ionization. The dynamics of CTTS-detached electrons in ammonia was found to be strongly affected by ion pairing. Geminate recombination time constants as well as escape probabilities were determined from the measured temporal profiles and analysed as a function of the medium density. A fast unresolved ($\tau < 250$ fs) increase of absorption related to the creation/thermalization of solvated electron species was followed by two decay components: one with a characteristic time around 10 ps, and a slower one that remains active for hundreds of picoseconds. While the first process is attributed to an early recombination of (I, e^-) pairs, the second decay and its asymptote reflects the effect of the K^+ counterion on the geminate recombination dynamics, rate and yield. The cation basically acts as an electron anchor that restricts the ejection distance, leading to solvent-separated counterion-electron species. The formation of (K^+, NH_3, e^-) pairs close to the parent iodine atom brings the electron escape probability to very low values. Transient spectra of the electron species have also been estimated as a function of time by probing the temporal profiles at different wavelengths.

Received 29th August 2017,
Accepted 31st October 2017

DOI: 10.1039/c7cp05903e

rsc.li/pccp

1. Introduction

The study of elementary charge transfer processes in solution using simple model systems contributes to the understanding of more complex reactions of this type that occur in many fields of chemistry and biology.[1–3] The first step of an intermolecular solvent-mediated charge transfer mechanism concerns electron ejection from the donor species into the solvent environment. Specific characteristics of the electron-solvent and electron-donor couplings, as well as the structural and transport properties of the host fluid, are the major factors determining the subsequent reactive channels.

The subpicosecond hydration dynamics of the electron has widely been studied since the pioneering pump–probe spectroscopic experiments performed years ago by the groups of Eisenthal[4–6] and Gauduel.[7] In these studies, electrons were released by ultraviolet (UV) multiphoton ionization (MPI) of (principally) neat water, or by photodetachment from simple anions in aqueous solution. The concentration of the species was commonly monitored by transient absorption (TA) in the near infrared (NIR) region of the spectrum. In particular, the laser-induced MPI of water was extensively studied at different excitation wavelengths, ranging from the adiabatic threshold to energies that surpass the conduction band of the fluid.[8–14] Interest in the ultrafast solvation dynamics of multiphoton ionized electrons was later extended to other hydrogen-bonding solvents such as alcohols.[15–18] Only very recently, the group of P. Vöhringer[19,20] performed the first successful femtosecond TA experiments capturing the dynamics of electrons in ammonia at different temperatures and densities. Ultrafast optical probing of fluid ammonia is a difficult task because it has to be carried out in a pressurized cell maintaining a constant temperature.

As mentioned above, a second way of injecting electrons in the solvent environment makes use of phototriggerable donors added to the fluid. Inorganic monoatomic halides[5,21–26] are simple electron donors commonly used in polar solvents, just as alkalides[3] were employed in nonpolar media. The electron transfer is initiated by photoexcitation of the donor species to a rather diffuse quasi-Rydberg state bound to the solvent field. The absorption bands that characterise such so-called charge-transfer-to-solvent (CTTS) transitions were extensively studied

[a] *DQIAQF-FCEN, Universidad de Buenos Aires and INQUIMAE-CONICET, Ciudad Universitaria, 3er piso, Pabellón II, Buenos Aires (C1428EGA), Argentina. E-mail: marceca@qi.fcen.uba.ar*

[b] *Department of Chemistry, University of Toronto, 27 King's College Circle, Toronto, Ontario (M5S 1A1), Canada*

† Present address: Department of Chemistry, University of Waterloo, 200 University Avenue West, Waterloo, Ontario (N2L3G1), Canada.

in the 70's for different systems by Blandamer and Fox.[27] CTTS-detached electrons are short-lived and thermalize within a few hundred femtoseconds into a series of non-equilibrium species. Thermalized electrons finally recombine with the donor *via* electron-radical annihilation, or eventually become solvated electrons.

In contrast with MPI, the energy required to generate electrons in a fluid doped with anionic donors is substantially lower. In particular, a single UV photon suffices to detach a 5p electron from iodide to the lowest CTTS band threshold. For example, the CTTS band's maxima for iodide in typical hydrogen bonding solvents are: 225 nm (water), ~220 nm (alcohols), and 260 nm (ammonia).[27] The detachment energy can be even lower when using sodide Na^- as a donor (λ_{max} = 730 nm),[28] although in this case a nonprotic solvent such as tetrahydrofuran (THF) has to be used.

For the iodide–water system, it is well established that the electrons produced by solvent relaxation of the lowest CTTS state exhibit a very different recombination dynamics from those injected into the conduction band of water by MPI.[29] Resonant CTTS excitation allocates the charge within the first water shells, which favours fast recombination. Based on quantum molecular dynamics simulations, the groups of P. Rossky[30] and D. Borgis[31] proposed years ago the formation of close-range halogen atom-electron pairs, of the type (I, e^-), acting as intermediate species in the recombination reaction of CTTS-detached electrons. In the model, the pairs may eventually regenerate the halide ion, *via* nonadiabatic recombination, or dissociate allowing the escape of free electrons into the fluid. The model perfectly reproduces the fast recombination rate measured in water, but needs to be expanded for more complex situations. One such case arises when more than a single relaxation time constant is involved in the kinetic mechanism, which unveils the presence of new intermediates. As an example, we will consider that the electrons were detached following CTTS excitation of I^- in a low-polarity solvent such as THF, extensively studied by the group of B. Schwartz.[24] For this system, it was shown that contact ion pairs (CIPs) of the type (Na^+, e^-) are formed due to mutual cation-electron diffusion, hindering the escape of electrons as free particles into the fluid. The low static dielectric constant of THF not only facilitates electron trapping as (Na^+, e^-) pairs, but also ensures tight proximity of Na^+ counterions to the electron ejection point. Indeed, (Na^+, I^-) CIPs are likely to be very abundant in THF solutions. The observed absorption transients were explained by the authors in terms of an electron-capture model, in which two different (~10 and ~100 ps) time constants were assigned to the formation of neighbouring or distant (Na^+, e^-) pairs, respectively. A portion of non-trapped electrons may still escape into the fluid and consequently a residual absorbance persists on subnanosecond time scales. The important effect of counterions on the electron dynamics in low dielectric solvents was demonstrated by the same group, repeating the experiments in the presence of a Na^+ complexing agent.[23] The formation of (Na^+, e^-) CIPs in a counterion-free environment was completely avoided, and almost all the electrons were able to escape into the solvent.

Ammonia and water are isoelectronic molecules, have similar dipole moments, and both are capable of forming intermolecular hydrogen bonding networks. Bearing in mind that CTTS excitation provides insufficient energy to reach the conduction band in either of these two liquid solvents,[29,32] an analogous dynamic behaviour could be expected in relation to host and solvate electrons. However, ammonia's static dielectric constant (ε_D) is substantially lower than that of water, and this would contribute to stabilizing counterion-electron pairing in this solvent, delaying electron recombination. In particular, the existence of solvent-separated ion pairs (SSIPs) between Na^+ and an ammoniated electron was corroborated by our group from the magnitude of the effective polarizability of isolated middle-size $Na(NH_3)_n$ clusters, measured by beam deflection.[33]

With ammonia being a highly structured polar liquid with poor charge separation capacity, the question that arises is: Which of these properties will govern the evolution of CTTS-detached electrons in the fluid? Despite the importance of liquid ammonia in the early studies of solvated electrons, there has been, to our knowledge, no study to date dealing with the ultrafast dynamics of CTTS-detached electrons in this solvent. In this work, we present TA experiments of electrons originating from CTTS excitation of a potassium iodide solution in liquid ammonia at different temperatures and densities. The results complement the MPI work carried out a few years ago by P. Vöhringer's group on neat ammonia.[19,20,32] Electron formation and recombination time constants, as well as escape probabilities, were derived from the measurements performed in the present study. Moreover, the time evolution of the transient absorption spectrum of the electron could be reconstructed from the temporal profiles probed at different wavelengths. In this paper, we highlight the differences and similarities observed among the dynamics of electrons in water, THF and ammonia.

2. Experimental section

2.1 Pump–probe transient absorption setup

Photodetachment and recombination dynamics of ammoniated iodide 5p electrons were studied by pump–probe ultrafast transient absorption. The measurements were performed on an optical cell that stands pressures up to p = 300 bar and temperatures up to T = 200 °C.

The laser system consists of a 1 kHz repetition rate chirped pulse amplification (CPA) regenerative amplifier, Coherent Legend Elite, seeded by an 80 MHz Ti:Sapphire oscillator, Coherent Micra 5, which delivers 100 fs (FWHM) laser pulses at λ_0 = 807 nm. An optical parametric amplifier, Coherent OPerA Solo, pumped by a fraction of the fundamental beam, delivered tuneable signal and idler NIR probe pulses covering the spectral region λ_2 = 1100–2200 nm. Five specific wavelengths (1150, 1370, 1580, 1760 and 2110 nm) were used in this work to probe the transient absorption of the electron species. The selected λ_2 wavelengths correspond to high-transmission spectral windows of dense ammonia—the fluid chosen in the present

work to host the iodide photoelectrons. They are sufficiently well distributed to probe most of the broad absorption band of the electron equilibrated in liquid NH_3 (absorption maximum at ~1760 nm and a spectral FWHM of ~1150 nm).[19] Gaussian temporal profiles were found suitable for describing the ultrafast NIR pulses at λ_2 = 1200 nm, characterized by a $FWHM_2$ = 80 fs measured by auto-correlation. The UV pump laser pulse centred at λ_1 = 269 nm was generated by frequency tripling a fraction of the 807 nm beam. Two 0.5-mm-thick β-BaB_2O_4 (BBO) crystals were employed for second- and third-harmonic generation. A 3.5 mm calcite plate was added after the first BBO crystal to compensate most of the group velocity mismatch of the fundamental and second-harmonic pulses propagating through the second crystal. The pulsewidth of the UV pump pulse was determined by performing a cross-correlation with the probe pulse (λ_2 = 1200 nm) on a 0.1-mm-thick type-II BBO crystal, and measuring the pulse duration of the resulting difference frequency generation beam ($\lambda_{1\times2}$ = 347 nm). The cross-correlation profile was satisfactorily fitted to a Gaussian curve with temporal $FWHM_{1\times2}$ = 247 fs, from which can be extracted a $FWHM_1$ = 234 fs for the pump pulse. The widths of UV and NIR pulses were insensitive to the presence of a 5-mm-thick single-crystal sapphire window, which was employed in the high-pressure optic cell. Moreover, the indetermination in the temporal superposition of the beams transmitted through the sample was considered negligible due to the small penetration of the UV light in the KI–NH_3 solution, *i.e.* an effective pathlength of *ca.* 30 μm, due to the high molar absorptivity of the iodide's CTTS band in ammonia, at 266 nm ($\varepsilon = 1.11 \times 10^4$ M^{-1} cm^{-1}).[34]

The optical layout of the setup allowed spatial-temporal overlap of the pump and probe pulses at the position of the cell containing the solution sample. The pump and probe beams were crossed with an angle of 3°. The UV beam was focused to a spot of 70 μm in diameter, using a fused silica lens with a 1 m focal length. The NIR beam was focused to 30 μm in diameter, using a 5 cm focal length CaF_2 lens. The probe pulse energy used in the experiments was 0.1 nJ and the pump pulse irradiance applied to the sample was ~20 GW cm^{-2}. Under such conditions it was found that the dominant electron detachment process proceeds *via* the lowest-lying CTTS state of the ammoniated iodide, excited by quasi-resonant single photon absorption (λ_{max} = 265 nm for the KI–NH_3 CTTS band at room temperature).[35] A competing two-photon channel producing a minor fraction of electrons could not be excluded from the experiment, either by increasing the KI concentration or by diminishing the pump irradiance to a tolerable signal-to-noise ratio. A precise control of the delay time between pump and probe pulses, $\tau = -0.01$ to 2 ns, was achieved by varying the pathlength of the NIR beam. To do this, we used a retroreflector mounted on a linear computer-controlled translation stage, with spatial resolution of 0.2 μm (equivalent to $\Delta\tau \approx 1$ fs, for a single reflection). The incident beam hitting the retroreflector was carefully aligned to minimize any angular variation in the reflected beam as the translation stage moved. Typically, the alignment procedure was considered satisfactory when, after a full scan ($\Delta\tau \approx 2$ ns), less than 5% intensity variation was measured behind a 50 μm pinhole on which the NIR laser was focused. The pinhole was located 4 m away from the retroreflector.

Laser fluctuation was minimized by implementing balanced detection of the probe signal using two identical InGaAs photodiodes (Thorlabs: FGA21 for $\lambda_2 < 1600$ nm, and DET10D/M for $\lambda_2 > 1600$ nm.). Before interacting with the cell, the NIR beam was split in two. A minor portion was used as a reference and its intensity was measured by one of the photodiodes (PD_{ref}). The rest of the beam (sample) was directed through the cell and the transmitted light was focused and quantified in the second photodiode (PD_{sample}). Reference and sample signals were conveniently amplified and integrated using boxcar averagers, leading, respectively, to the intensities i_{ref} and i_{sample}. Next, an analogue voltage divider was employed to normalize the sample intensity by the reference, producing a shot-by-shot signal proportional to the ratio i_{sample}/i_{ref}. Pump-on/pump-off modulation of this signal was achieved using a mechanical chopper, synchronized with the repetition rate of the laser, which blocked every other UV excitation pulse. The pump-on/pump-off sequence of i_{sample}/i_{ref} values was then digitalized in a computer by means of a 16-bit resolution acquisition card, and the transient absorbance of the solution ΔA (in units of optical density) was calculated by taking the ratio of two consecutive pulses, as:

$$\Delta A\ (\mathrm{OD}) = -\log \frac{\left(i_{sample}/i_{ref}\right)_{pump\text{-}on}}{\left(i_{sample}/i_{ref}\right)_{pump\text{-}off}} \qquad (1)$$

The values of ΔA were therefore evaluated at half of the repetition rate of the laser (0.5 kHz duty cycle).[36] Typically, an adequate signal-to-noise ratio was attained by averaging 500 values of ΔA calculated using eqn (1) before stepping the translation stage to the next position. Finally, 16 replicas of the full temporal profiles were added together and normalized. Following the aforementioned procedure, TA signals as low as 2 mOD could be measured with our setup. All the TA profiles collected in this work were found to be unaffected by the relative polarization between the pump and probe beams, controlled by means of a half-wave plate positioned in the UV arm of the apparatus.

2.2 Optical cell and ancillary loading equipment

The optical cell body was constructed in stainless steel, against which 5-mm-thick sapphire windows were tight sealed using gold foils. The KI–NH_3 solution was forced to diffuse through the 800 μm pathlength of the cell by means of a magnetic stirrer located below the beam height. We verified that the refreshment of liquid in the optical channel of the cell was good enough to avoid the accumulation of photoproducts during the measurements. To do this, the repetition rate of the experiment was decreased from 500 to 60 Hz without evidencing changes in the TA profile of a given KI–NH_3 solution. A fresh sample was synthesized in the cell in most of the measurements. The temperature of the cell was maintained at the desired value within ±0.1 K using electric heaters controlled by a PID system, and measured using calibrated Pt thermometers. A pressure transducer continuously monitored the pressure in the cell

with an uncertainty of ±0.1 bar. The salt concentration selected in the experiments was 100 mM in KI. The solutions were prepared directly in the optical cell using ancillary gas handling equipment. To do this, 50.0 mg of crystalline KI was introduced into the cell and the system was maintained under vacuum at 60 °C for one day to dry the solid and remove the air. Next, 3.0 cm^3 of dry ammonia (99.99% purity) was carefully distilled into the cell. By following this procedure, the liquid solution occupied most of the internal volume of the cell, leaving a small vapour bubble on the top. The cell was finally isolated from the loading equipment by means of a high-pressure needle valve.

2.3 Sampled experimental region

The measurements were performed at a constant KI molar concentration and different temperatures (298, 313, 333, 353 and 373 K), along the liquid–vapour coexistence curve of the KI–NH_3 mixture. For each experimental condition, the molar density of pure ammonia (ρ_{sat}), calculated by applying the equation of state proposed by L. Haar *et al.*,[37] was taken as an estimation of the density of the liquid solution. This assumption only leads to a ~2% underestimation in the density values given in Table 1, based on former density measurements performed on ~100 mM KI–NH_3 solutions at 241 K.[38]

3. Results

3.1 Transient absorption profiles

In Fig. 1 we show a representative transient absorption profile of the iodide solution in liquid ammonia at T = 298 K (ρ_{sat} = 35.4 M), excited at λ_1 = 269 nm and probed at λ_2 = 1370 nm. The inset provides a detailed description of the first 25 ps of the dynamics. The general features of the TA profiles are preserved at all fluid densities. Several species associated with the released electron would in principle contribute to the absorption signal. We will see later that these include pre-solvated, fully ammoniated, counterion-paired, and parent

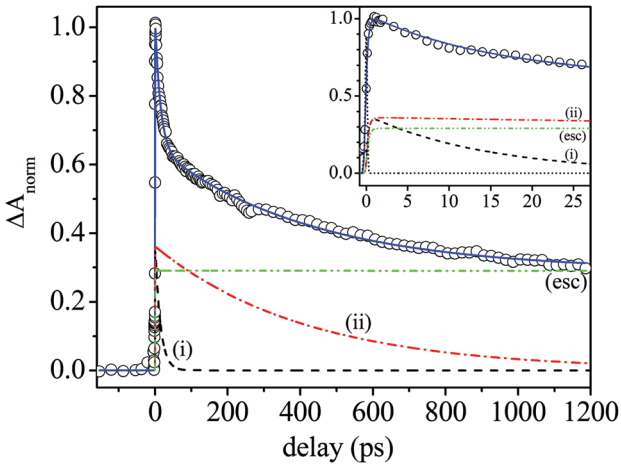

Fig. 1 Normalized ultrafast transient absorption profile $\Delta A_{norm} = \Delta A/a_{max}$ of a 100 mM solution of KI in saturated liquid ammonia at T = 298 K (ρ_{sat} = 35.4 M). Pump and probe wavelengths: λ_1 = 269 nm and λ_2 = 1370 nm. Experimental data: symbols. Overall increase/decay fit: solid line. Exponential components: earlier dynamics (i), longer timescale dynamics (ii), escape (esc) probability P_{esc} = 27%. Gaussian response of the apparatus: short dashes. Inset: First few picoseconds of the transient absorption profile.

Table 1 Parameter list corresponding to the fitting of the normalized profiles, for the different experimental conditions. (Estimated values are indicated by asterisks)

T (K)	ρ_{sat} (M)	τ_i (ps)	τ_{ii} (ps)	P_i (%)	P_{ii} (%)	$\frac{P_i}{P_i + P_{ii}}$	P_{esc}^{1P+2P} (%)	P_{esc}^{1P*} (%)
λ_1 = 269 nm, λ_2 = 1150 nm								
298	35.4	11.6	323	37	30	0.54	33	16
313	34.1	9.2	292	40	34	0.54	26	12
333	32.0	7.2	178	41	36	0.53	23	7
353	29.7	7.4	190	44	37	0.54	19	3
373	26.9	6.6	151	47	38	0.55	15	1
λ_1 = 269 nm, λ_2 = 1370 nm								
298	35.4	14.5	420	37	35	0.51	28	16
313	34.1	12.3	300	40	35	0.53	25	12
333	32.0	14.2	281	39	40	0.49	21	7
353	29.7	11.7	243	41	42	0.49	17	3
373	26.9	11.4	263	43	42	0.51	15	1
λ_1 = 269 nm, λ_2 = 1580 nm								
298	35.4	17.2	435	35	37	0.49	28	16
313	34.1	16.2	332	36	41	0.47	23	12
333	32.0	13.3	305	38	40	0.49	22	7
353	29.7	13.9	300	40	42	0.49	18	3
373	26.9	13.7	301	41	42	0.49	17	1
λ_1 = 269 nm, λ_2 = 1760 nm								
298	35.4	9.4	500	25	40	0.39	35	16
λ_1 = 269 nm, λ_2 = 2110 nm								
298	35.4	8.0	481	25	35	0.42	40	16

atom-paired electrons. The function (solid line) used to fit the data (symbols) consists of a sum of one mono-exponential increase, two mono-exponential decays, and an additional infinite time response exponential that accounts for the observed residual absorbance. The four terms of the fitting function are convoluted with the response function of the apparatus, the latter being approximated by the Gaussian fit of the UV/NIR cross-correlation. The origin of the delay time coordinate ($t = 0$) resulting from the fit corresponds physically to the temporal overlap of the pump and probe pulses at the sample volume. At $t = 0$, the pump induced absorption shows a fast increase in all the profiles, with a characteristic time limited by the temporal resolution of the apparatus (τ_{rise} always smaller than 0.25 ps in the fitting procedure). This observation is compatible with previous TA studies of electrons detached from iodide CTTS states in other polar solvents, such as water[21,39] and ethylene glycol,[29] where the appearance time was found to be ~200 fs. Such a rapid increase in the probe absorption signal was also found when the electrons were generated by two-photon ionization of neat liquids; for example, ammonia[19] and water.[29]

3.2 Fitting procedure

The electron/water relaxation model proposed by Rossky[30] and Borgis[31] is unsuccessful in the iodide-ammonia case because it cannot account for the two clear decay components observed in the TA profiles. In a first approximation, we can speculate that the total amount of electrons injected in the fluid at $t = 0$ is distributed among three competitive channels. Their branching ratios are given by the following equation: $a_{max} = a_i + a_{ii} + a_{esc}$, where a_{max} is the TA at the profile's maximum, a_i and a_{ii} represent the amplitudes of two distinct decay channels, and a_{esc} corresponds to the residual absorbance that persists during the time scale of the experiment. The decay processes (i) and (ii) in Fig. 1 account respectively for a fast geminate annihilation and a longer timescale recombination, while the residual absorbance (esc) represents the presence of long-living electrons that escaped from encountering the parent iodide radical. The three contributions to the TA decay are plotted individually in Fig. 1, each one of them convoluted with the time response of the apparatus. In the conditions of this particular experiment, only a minor part of the electrons injected in the fluid were able to escape from picosecond-scale recombination, with an escape probability: $P_{esc} = 100 \times a_{esc}/a_{max} = 27\%$. The rest of the electrons decayed exponentially using either the first (time constant $\tau_i = 14$ ps) or second mechanism ($\tau_{ii} = 416$ ps), with similar yields: $P_i = 100 \times a_i/a_{max} = 38\%$ and $P_{ii} = 100 \times a_{ii}/a_{max} = 35\%$, respectively.

3.3 Temperature and density dependence of the profiles

Iodide-ammonia normalized TA profiles are displayed in Fig. 2 for five different temperatures at three probe wavelengths, emphasizing the first picoseconds of the dynamics in the insets. The saturation densities of the fluids corresponding to each temperature are tabulated in Table 1. The main feature observed in Fig. 2 for each constant-λ_2 series is the growth of

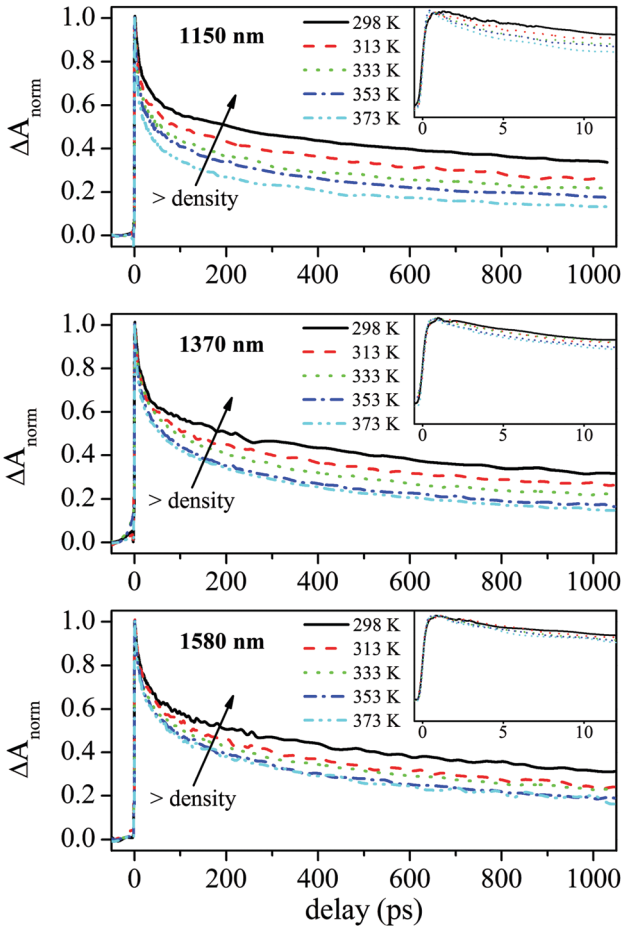

Fig. 2 Temperature dependence of the normalized transient absorption $\Delta A_{norm} = \Delta A/a_{max}$ of 100 mM KI in saturated liquid ammonia at probe wavelengths λ_2 = 1150 nm, 1370 nm and 1580 nm (λ_1 = 269 nm). Experimental data are connected by lines. An extended temporal scale is shown in the insets.

the escape probability by decreasing the temperature (from ~15% to ~30% residual absorbance on going from 373 K to 298 K). We will see later that this effect is better explained in terms of the concomitant increase in the molar density of the fluid, which favours the electron trapping in solvent cavities.

The values of the parameters τ_i, P_i, τ_{ii}, P_{ii}, and P_{esc}^{1P+2P}, resulting from the fitting of all the measured profiles, are tabulated in Table 1, labelled by the (T, ρ_{sat}) conditions of each experiment. However, before analysing their temperature/density variation in detail, it is convenient to establish the number of photons involved in the production of electrons in the fluid.

3.4 Number of UV photons absorbed

In Fig. 3 the transient absorbance maximum of a 100 mM KI–NH_3 solution is plotted as a function of the pump laser irradiance, I, maintaining the rest of the conditions identical to those of Fig. 1. The subtle but clear parabolic behaviour of ΔA_{max} *vs.* I indicates that the transient concentration of electrons in the solution, considering all the absorbing species, originates in two competing channels. They correspond to

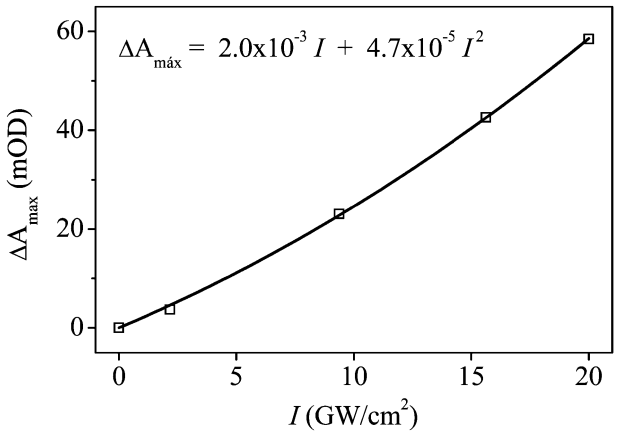

Fig. 3 Dependence of the transient absorbance maximum ΔA_{max} with the pump laser irradiance I, in a 100 mM KI–NH_3 solution at T = 298 K (ρ_{sat} = 35.4 M), pumped at λ_1 = 269 nm and probed at λ_2 = 1370 nm. Single- and two-photon contributions assumed simple power laws on the irradiance.

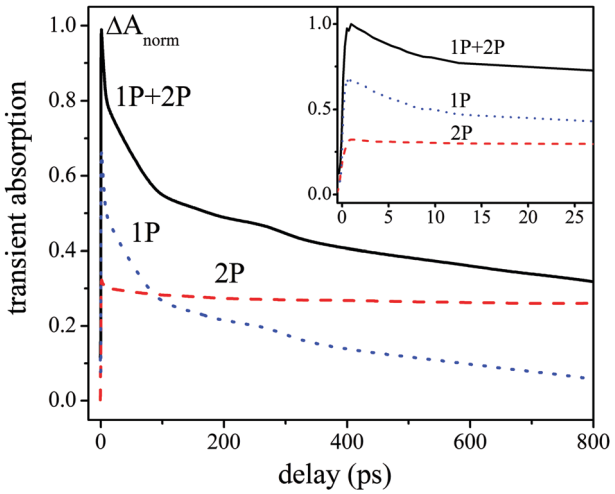

Fig. 4 One- (1P) and two-photon (2P) ionization components of a 100 mM KI–NH_3 TA profile (1P + 2P) [T = 298 K, ρ_{sat} = 35.4 M ≡ 0.60 g cm^{-3}, λ_1 = 269 nm, λ_2 = 1370 nm]. 2P contribution taken from ref. 19 for neat NH_3 under similar conditions [T = 258 K, ρ = 0.68 g cm^{-3}, λ_1 = 2 × 266 nm, λ_2 = 1450 nm], multiplied by the branching ratio 0.32. The 1P contribution was calculated by subtraction.

single- (1P) or two-photon (2P) ionization mechanisms. Therefore, the temporal evolution of ΔA can be written as:[40]

$$\Delta A(t, I) = \Omega_{1P}(t)\sigma_{1P}I + \Omega_{2P}(t)\sigma_{2P}I^2 \quad (2)$$

where $\Omega_{nP}(t)$ represents the electron survival probability at time t, and σ_{nP} is the effective cross-section for the n-photon (n = 1P or 2P) ionization mechanism. The parabolic fit shown in Fig. 3 allowed us to evaluate the effective cross sections σ_{1P} = 2.0 × 10^{-3} cm^2 GW^{-1} and σ_{2P} = 4.7 × 10^{-5} cm^4 GW^{-2}, since at ΔA_{max} both Ω_{1P} and Ω_{2P} are equal to one. The branching ratio for the 1P and 2P ionization channels can therefore be estimated using eqn (2). For the UV laser irradiance used in the experiments and the fluid density ρ_{sat} = 35.4 M, the normalized absorbance at time t is given by: $\Delta A_{norm}(t)$ = 0.68 × $\Omega_{1P}(t)$ + 0.32 × $\Omega_{2P}(t)$. Hence, two electron processes are driven under our experimental conditions: (i) a major fraction (68%) is generated *via* single-photon CTTS excitation, and (ii) a smaller fraction (32%) is generated by absorption of two UV photons, resembling the 266 nm two-photon ionization experiments performed by Vöhringer's group in neat liquid NH_3.[19,20] Interestingly, the competing 2PI channel is no longer present if the solvent is changed to methanol under exactly the same experimental conditions, revealing the smaller σ_{1P}/σ_{2P} cross section ratio in the case of ammonia. An attempt to disentangle the 1P and 2P contributions is shown in Fig. 4 for a representative TA profile (100 mM KI–NH_3 solution, T = 298 K, ρ_{sat} = 35.4 M). The two-photon contribution (represented by a dashed line) was taken from ref. 19 and scaled by a factor of 0.32 to match the branching ratio imposed by eqn (2). The 1P component (dotted line) was calculated by subtraction between the experimental profile and the scaled 2P contribution, namely 0.68 × $\Omega_{1P}(t)$ = $\Delta A_{norm}(t)$ − 0.32 × $\Omega_{2P}(t)$. As shown in Fig. 4, the concentration of electrons generated by two-photon ionization exhibits a subpicosecond increase and then drops very slowly during the first nanosecond of the dynamics (∼6%). Such quasi step-function behaviour of the 2P contribution to the dynamics lets us assume that both the short- and long-timescale decays following CTTS photoexcitation would still reasonably be captured by the parameters τ_i, P_i, τ_{ii}, and P_{ii} given in Table 1.

According to the behaviour at long delay times visualized in Fig. 4, it can be concluded that the 2P component of the profile accounts for most of the observed escape probability (P_{esc}^{1P+2P} in Table 1). However, a small but appreciable contribution of the 1P channel would also be expected from the tendency of the curves in Fig. 4. With the purpose of analysing whether this effect depends on the fluid density, the tabulated P_{esc}^{1P+2P} values were plotted in Fig. 5 together with the 2P escape probability observed for neat ammonia.[19] The 2P contribution to the escape, indicated as P_{esc}^{2P} in Fig. 5, was scaled by a factor of 0.32 to match the branching ratio imposed by eqn (2). It is observed that all the constant-λ_2 series have a common general tendency, increasing P_{esc}^{1P+2P} more steeply with density than the 2P component. By subtraction, it is possible to estimate a trend for the escape probability expected for one-photon CTTS electrons, being 0.68 × P_{esc}^{1P} = P_{esc}^{1P+2P} − 0.32 × P_{esc}^{2P}. The estimated density dependence of P_{esc}^{1P} is shown in Table 1. When liquid density is below 27 M, there are practically no CTTS electrons that manage to escape into the solvent. For higher densities, the 1P escape probability increases gently, reaching a value of ∼15% at ρ_{sat} = 35 M (density of liquid ammonia at room temperature).‡

We stated that the data collected under the conditions of our experiment cannot exclusively be attributed to electrons originated in the relaxation of CTTS states, because they are partly obscured by a 2P detachment channel into the conduction band of NH_3. However, due to the smooth time dependence of

‡ In the former analysis, we left out temperature differences between the experimental series in ref. 19 and those in the present work, relying on the use of ρ as the most relevant variable.

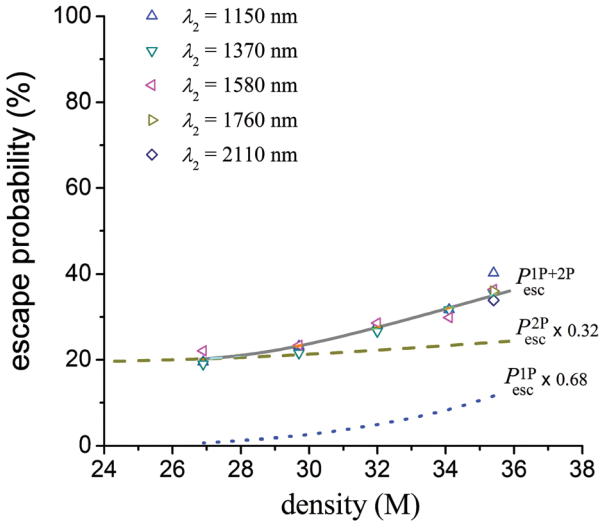

Fig. 5 Escape probability of electrons detached from a 100 mM solution of KI in ammonia at T = 298 K, as a function of the saturation density (λ_1 = 269 nm). Symbols: data measured at different probe wavelengths λ_2 (solid line drawn to guide the eyes). Dashed curve: 2PI escape measured in ref. 19. Dotted line: 1P contribution to the escape was estimated by difference. 1P and 2P contributions were scaled according to eqn (2).

the 2P channel shown in Fig. 4, we will assume in a preliminary analysis that the parameters τ_i and τ_{ii} reasonably represent the two competitive decay constants of 1P CTTS electrons. The relative ratio between these two channels is given by the ratio $P_i/(P_i + P_{ii})$ in Table 1. In the same table, the magnitude P^{1P}_{esc} gives us an estimation of how many electrons following CTTS excitation avoid recombination and become free solvated particles.

4. Discussion

4.1 Ion pairing in liquid ammonia

We will start by analysing the speciation of a 100 mM solution of KI in liquid ammonia under the conditions of the present experiment. According to the primitive model of electrolyte solutions, a medium with a relatively low value of the product ($T\varepsilon_D$) will favour the association of ions with opposite charge. However, it is a well-known fact that the formation of contact (or "tight") ion pairs does not entirely explain the observed phenomena[41–43] and another type of species (characterised as solvent-separated or "loose" ion pairs) may exist in the solution. Moreover, it has been proposed[44] that ion pairing proceeds in steps *via* two ionic association equilibria, according to:

$$M^+_{sv} + X^-_{sv} \xrightarrow{1} (M^+\ sv, X^-)_{sv} \xrightarrow{2} (M^+, X^-)_{sv} \qquad (3)$$

where reactions (1) and (2) represent the formation of SSIPs and CIPs, respectively, for a 1 : 1 electrolyte MX, and (sv) indicates a solvated species. Conductivity measurements performed years ago[45] on the KI–NH_3 system at T = 239 K and under saturation pressure showed that KI behaves as a moderately weak electrolyte in this solvent, reporting an overall ion association constant K_a^{239K} = 246 (in the molarity scale). Earlier stationary UV spectra performed in our laboratory[35] on KI–NH_3 solutions, over a range of temperatures at liquid–vapour equilibrium, enabled us to discriminate between the absorbance of (K^+, I^-) CIPs from the other absorbing species. The analysis of these results revealed that the presence of CIPs was only appreciable at temperatures above 350 K, and therefore it seems reasonable to consider in the present study that free I^- ions and (K^+, NH_3, I^-) SSIPs are the only two absorbing species. The overall ion association constant can thus be approximated by that of the first equilibrium step in (3), as:

$$K_a \approx K_1 = \frac{(1-\alpha)}{\alpha C}\frac{1}{\gamma^{\pm 2}} \qquad (4)$$

where α is the degree of dissociation of KI, $\gamma^{\pm}$ is the mean activity coefficient of the ammoniated free ions, and C is the salt concentration. We used Bjerrum's theory,[46] which is the natural extension of the Debye–Hückel theory for ionic association, to estimate the value of K_a over the range of temperatures in the present study. To do this, the average distance of closest approach of ions in the SSIP was set to 0.6 nm on the basis of earlier molecular dynamics simulation runs,[35] and the dielectric constant of NH_3 was taken from ref. 47. At T = 298 K ($T\varepsilon_D$ = 5070), the calculated value for $K^{298K}_{a,calc}$ is 244, which is very similar to the experimental value reported at T = 239 K (K_a^{239K} = 246, $T\varepsilon_D$ = 5000),[41] while at T = 373 K ($T\varepsilon_D$ = 3360) $K^{373K}_{a,calc}$ = 2080. Using the extended Debye–Hückel equation to evaluate the mean activity coefficient, the degree of dissociation of KI can finally be determined by employing eqn (4) leading to α = 0.54 at T = 298 K and α = 0.45 at T = 373 K. In other words, in the present experiment approximately half of the CTTS electrons were detached from free iodide ions while the other half were detached from (K^+, NH_3, I^-) SSIPs, the latter being the electrons strongly affected by the proximity of the K^+ counterion.

4.2 Ejection and recombination dynamics

The temporal resolution of our instrument only lets us establish an upper limit of ~250 fs to the electron signal growth. Such a steep increase is not exclusive of electrons detached from ammoniated iodide ions, since the same was observed by direct two-photon ionization of the same solvent.[19] The fast electron detachment in NH_3 and the weak dependence on the ejection mechanism were also found in aqueous systems, where a ~200 fs signal increase was reported either for CTTS photoexcitation of iodide solutions or direct ionization of water.[29] For comparison, a slower increase (~380 fs) was observed for iodide ions in the non-protic solvent THF.[23]

We have stated that electrons detached from CTTS states in ammonia are much more likely to recombine than those generated by 2PI in neat NH_3. For example, at ρ_{sat} = 35.4 M, ~84% of CTTS electrons recombine within the first nanosecond (P^{1P}_{esc} = 16% in Table 1) while only ~20% can do it in the case of 2PI electrons.[19] The larger recombination yield of CTTS electrons may in principle be associated with a smaller ejection distance from the parent iodine atom. In the present experiments, the pump wavelength (λ_1 = 269 nm ≡ 4.61 eV) was very close to the iodide CTTS band's maximum, independent of

being a free ammoniated ion or belonging to a SSIP,[35] and only slightly above the resonant energy threshold. The CTTS band's maximum is located at λ_{max} = 266–275 nm (4.66–4.51 eV) when going from 298 K to 373 K,[35,48] and the band onset is at 300 nm ≡ 4.13 eV.[48] Hence, the limited excess energy deposited on the electrons upon excitation would in principle restrict the ejection distance to the first solvent shells, depending on the instantaneous solvent structure. Moreover, we can hypothesize that when the electron is detached from a free ammoniated iodide ion, it will quickly be stabilised as a (I, e^-) pair similar to the case of aqueous systems.[30,31] If, instead, the electron is detached from an (K^+, NH_3, I^-) SSIP, it may rapidly be captured by the nearby K^+ counterion leading to a (K^+, NH_3, e^-) moiety, which can also be viewed as an SSIP. Counterion-electron species have also been detected in NaI–THF solutions by the group of B. Schwartz,[24] where the authors demonstrate the dominant role of (Na^+, e^-) CIPs in electron dynamics. In NH_3, however, the concentration of cation-electron CIPs is expected to be very low at liquid densities,[35] with SSIPs instead being the potential species that may be involved in the electron dynamics. Moreover, (Na^+, NH_3, e^-) SSIPs have recently been found in ammonia clusters doped with a sodium atom, where the 3s electron of the metal is spontaneously transferred to the first solvent shells, interacting with the alkaline cation.[33] Based on the aforementioned evidence, it seems reasonable to postulate that quite stable (K^+, NH_3, e^-) pairs are formed upon electron detachment from (K^+, NH_3, I^-) SSIPs. If the preceding interpretation is correct, the overall recombination time constant will essentially be limited by the lifetime of the transient species (I, e^-) or (K^+, NH_3, e^-).

It is worth comparing the TA profiles obtained in liquid ammonia with those measured in water, where counterion-electron species are absent. In the iodide–water system, it takes approximately 150 ps for the TA signal to reach the residual absorbance that accounts for the escaped electrons,[29,49] while the decay time extends to ~1 ns for iodide-ammonia (see Fig. 2). Why is the recombination rate of CTTS-detached electrons slower in ammonia? Contrasting the evidence collected in water–ethylene glycol mixtures,[29] longer decay times in ammonia cannot be explained as a viscosity effect on the I–e^- mutual diffusion coefficient. This is simply because the bulk viscosity of NH_3 is about 7 times smaller than that of H_2O at room temperature. Moreover, the slower I–e^- encounter dynamics in liquid ammonia *vs.* that in water seems unrelated to the relative magnitude of the bulk diffusion coefficient for the electron in these solvents. In fact, it is known that the excess electron mobility is considerably larger in ammonia,[50] *i.e.* D_{e^-,H_2O}= 0.5 × 10^{-4} cm^2 × s^{-1} at 298 K[51] *vs.* D_{e^-,NH_3} = 1.5 × 10^{-4} cm^2 × s^{-1} at 223 K,[52] and we expect this value to be even larger at 298 K. Once the long-range solvent effects can be ruled out, the subnanosecond timescale of electron recombination in ammonia seems better connected to the formation of (K^+, NH_3, e^-) species in the solution with similar lifetimes. We will see in Section 4.3 that counterion-electron pairs absorb in the same spectral region as the free ammoniated electron and consequently their presence slows down the overall signal decay.

Based on the previous discussion, we will provide a plausible assignation to the two recombination channels described in Table 1. To simplify the analysis, we will first focalize in the data within each series at a constant probe wavelength and address the spectral details in Section 4.3. Channel (i) involves a fast electron-iodine atom radical annihilation with a characteristic time of, for example, 17 ps at 298 K (probed near the absorption maximum). This channel is driven by electrons that separate from the CTTS state of free I^- ions leading to (I, e^-) pairs. According to the model proposed by Rossky[30] and Borgis,[31] the observed decay results from a subtle competition between two processes: escape of electrons into the fluid *vs.* electron-iodine atom recombination to regenerate I^- in the ground state. The energy barrier that electrons must overcome before escaping into the fluid is high enough to maintain P_{esc}^{1P} at very small values, particularly when the density is low (see Fig. 5). In contrast, channel (ii) is a recombination pathway that lasts hundreds of picoseconds and involves the CTTS electrons that were detached from (K^+, NH_3, I^-) SSIPs. The detached electron is trapped by the nearby counterion, leading to a stable (K^+, NH_3, e^-) structure that delays recombination. The fraction of electrons decaying along mechanisms (i) and (ii), given by the value of $P_i/(P_i + P_{ii})$ in Table 1, is always close to 0.5, independent of the fluid density. This is compatible with the values estimated for the degree of dissociation of KI in NH_3. Within each λ_2-series, Table 1 shows a slowing down in both recombination channels (longer τ_i and τ_{ii} values) by lowering T. For an entirely thermal effect, both channels are found to be moderately activated according to Arrhenius plots, with activation energies lower than 7 kJ × mol^{-1}.

4.3 Spectral response

In a first approximation, the spectral evolution of the electron species in liquid ammonia at T = 298 K can be reconstructed from the temporal profiles probed at five specific wavelengths, distributed on the red and blue sides of the absorption's maximum of the equilibrated electron in ammonia. The data are plotted in Fig. 6a, where each one of the profiles has been scaled to match the long time (1.2 ns) absorbance with that of the stationary spectrum of the ammoniated electron.[19] The scaling mitigates slight variations in beam superposition and focusing conditions arising from tuning the probe wavelength in the OPA. The five temporal profiles intersected at defined delays (indicated by dotted lines in Fig. 6a) generate approximate transient spectra of the electron species (Fig. 6b). The absorption bands are at least 800 nm (FWHM), evidencing a tail that extends to the red, which resembles the stationary absorption spectrum of ammoniated electrons in Na–NH_3 liquid solution.[53]

Despite water and ammonia belonging to the same family of liquids (both being polar and capable of forming hydrogen-bonding networks), the transient spectra of CTTS electrons are quite dissimilar in these two solvents. First, the blue shift that characterises the early absorption of iodide-detached electrons in water is not present in ammonia (or it is obscured by our insufficient temporal resolution). Moreover, the spectral evolution to the blue in water ceases completely in the first 10 ps,[54]

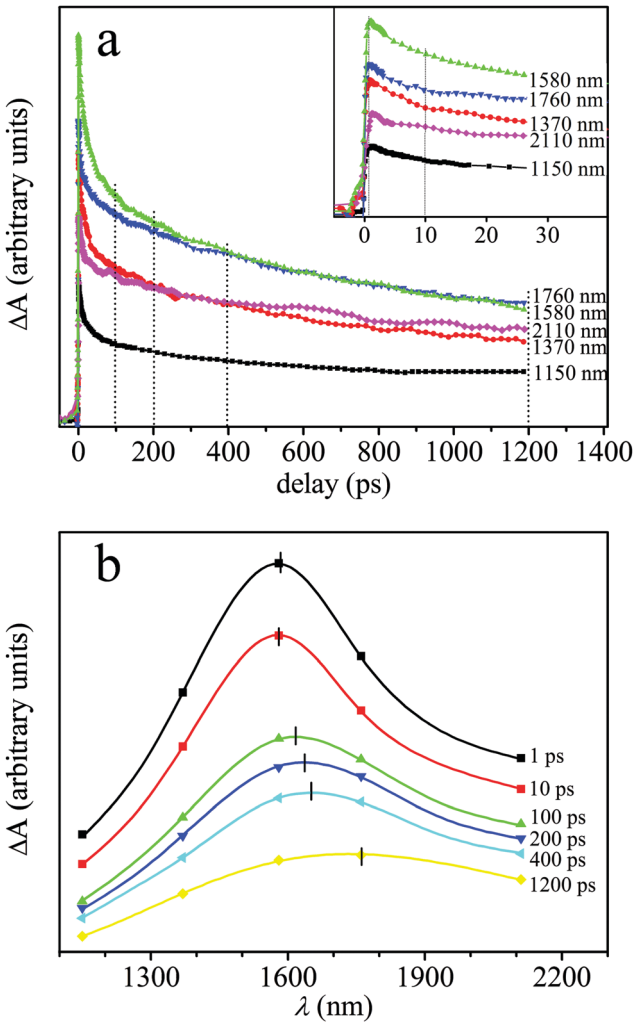

Fig. 6 Transient absorption ΔA of 100 mM KI in saturated liquid ammonia at T = 298 K (ρ_{sat} = 35.4 M) pumped at λ_1 = 269 nm. Data (symbols). (a) rescaled profiles (5 different probe wavelengths), the absorbance at 1.2 ns delay matches that of the equilibrated electrons in neat ammonia, generated by 2 × 266 nm ionization.[19] (b) Transient spectra of electrons obtained by interpolating the absorption profiles at selected delay times (dotted lines in panel a). Curves were drawn to guide the eyes. Ticks indicate the absorption's maxima.

while in ammonia a red shift lasts several hundreds of picoseconds (see Fig. 6b). The absorption's maximum of CTTS electrons in NH_3 shifts from 1580 nm (τ < 20 ps) to 1760 nm ($\tau \approx 1$ ns), corresponding to λ_{max} of the ammoniated electron.[19] Such spectral differences originate from the distinct absorbers existing in each solvent. For example, counterion-electron species in ammonia, which are expected to absorb at slightly higher energies than free electrons, can account for the long-lasting red shift. A similar spectral feature is found in THF, where ion pairing is known to participate in the recombination dynamics.[24] For example, Na^+-electron pairs in THF also appear at higher energies (~1250 nm blue-shifted) than the solvated electron,[55,56] evidencing a strong stabilization. Moreover, looser Na^+-electron pairs characterised by a larger separation are also present in THF, albeit with a smaller spectral shift.[24] Assuming that the spectrum of such loose pairs would not be so different from that of an electron detached from a tetrabutylammonium iodide solution, the same authors estimated that the absorption of loose Na^+-electron pairs in THF is 450 nm blue-shifted from that of the solvated electron. A similar spectroscopic behaviour (~180 nm blue shift) is evidenced in Fig. 6b for (K^+, NH_3, e^-) SSIPs in NH_3.

5. Conclusions

We have performed transient absorption experiments on electrons originate from CTTS excitation of ammoniated iodide in close proximity to the counterion at different saturation liquid densities. The collected data are compatible with competitive and very fast electron detachment from ammoniated free iodide anions and (K^+, NH_3, I^-) SSIPs, which are abundant species in the solution. Electron ejection proceeds *via* either a one-photon CTTS excitation or a two-photon mechanism. It was assumed that the 2P channel behaves like in previous MPI studies in neat ammonia.[19] These data were used to extract the 1P contribution to the escape probability from the measured profiles in Fig. 2, and interpret correctly the fitted decay parameters listed in Table 1.

Like in water, the ejection of electrons in ammonia following CTTS excitation of iodide is fast, with a characteristic time shorter than the temporal resolution of our apparatus. Since in the experiment the excitation was quasi-resonant, electrons detached with low kinetic energies are very likely thermalized within the first solvent shells. However, in spite of the proximity between the parent iodine atom and the CTTS electron, we observed that recombination lasts much longer in ammonia (~1 ns) than in water (~150 ps). Although a first recombination mechanism with a characteristic time of a few picoseconds is present in both solvents, a new longer timescale channel appears in ammonia revealing the effect of the K^+ counterion on the dynamics. We believe that, mimicking the behaviour in water,[30,31] the first channel involves electron detachment from free iodide ions leading to (I, e^-) pairs, which can later dissociate and yield solvated electrons or recombine to regenerate I^- *via* a nonadiabatic path. Instead, the second channel concerns electrons detached from (K^+, NH_3, I^-) SSIPs, which are trapped by the nearby counterion leading to stable (K^+, NH_3, e^-) pairs that delay the geminate recombination dynamics. The two channels are found to compete with each other because, according to the primitive model of electrolyte solutions, both free iodide and (K^+, NH_3, I^-) SSIP are very abundant in liquid ammonia.

Finally, we were able to estimate the transient absorption spectra as a function of time (Fig. 6b). We observed that the absorption band experiences a notorious red-shift *vs.* time, which is compatible with the existence of (K^+, NH_3, e^-) intermediates in the solution.

Conflicts of interest

There are no conflicts to declare.

Acknowledgements

We are grateful for partial economic support given by UBACyT 20020100100514, CONICET PIP 378, and FONCyT PICT 1314/2011. E. M. is a member of Carrera del Investigador, CONICET (Argentina). The authors thank Prof. L. Trevani (Univ. of Ontario Institute of Technology) and Prof. G. Sciaini (Univ. of Waterloo) for very useful discussions.

Notes and references

1 R. A. Marcus and N. Sutin, Electron Transfers in Chemistry and Biology, *Biochim. Phys. Acta*, 1985, **811**, 265–322.
2 P. F. Barbara, T. J. Meyer and M. A. Ratner, Contemporary Issues in Electron Transfer Research, *J. Phys. Chem.*, 1996, **100**, 13148–13168.
3 I. B. Martini, E. R. Barthel and B. J. Schwartz, Optical Control of Electrons During Electron Transfer, *Science*, 2001, **293**, 462–465.
4 F. H. Long, H. Lu and K. B. Eisenthal, Femtosecond Studies of Electron Photodetachment of Simple Ions in Liquid Water: Solvation and Geminate Recombination Dynamics, *J. Chem. Phys.*, 1989, **91**, 4413–4414.
5 F. H. Long, H. Lu, X. Shi and K. B. Eisenthal, Femtosecond Studies of Electron Photodetachment from an Iodide Ion in Solution: The Trapped Electron, *Chem. Phys. Lett.*, 1990, **169**, 165–171.
6 F. H. Long, H. Lu and K. B. Eisenthal, Femtosecond Studies of the Presolvated Electron: An Excited State of the Solvated Electron?, *Phys. Rev. Lett.*, 1990, **64**, 1469–1472.
7 Y. Gauduel, S. Pommeret, A. Migus, N. Yamada and A. Antonetti, Femtosecond Investigation of Single-Electron Transfer and Radical Reactions in Aqueous Media and Bioaggregate-Mimetic Systems, *J. Opt. Soc. Am. B*, 1990, **7**, 1528–1539.
8 R. A. Crowell and D. M. Bartels, Multiphoton Ionization of Liquid Water with 3.0–5.0 eV Photons, *J. Phys. Chem.*, 1996, **100**, 17940–17949.
9 R. Laenen, T. Roth and A. Laubereau, Novel Precursors of Solvated Electrons in Water: Evidence for a Charge Transfer Process, *Phys. Rev. Lett.*, 2000, **85**, 50–53.
10 A. Hertwig, H. Hippler and A.-N. Unterreiner, Temperature-Dependent Studies of Solvated Electrons in Liquid Water with Two and Three Femtosecond Pulse Sequences, *Phys. Chem. Chem. Phys.*, 2002, **4**, 4412–4419.
11 P. Kambhampati, D. H. Son, T. W. Kee and P. F. Barbara, Solvation Dynamics of the Hydrated Electron Depends on Its Initial Degree of Electron Delocalization, *J. Phys. Chem. A*, 2002, **106**, 2374–2378.
12 Q.-B. Lu, J. S. Baskin and A. H. Zewail, The Presolvated Electron in Water: Can It Be Scavenged at Long Range?, *J. Phys. Chem. B*, 2004, **108**, 10509–10514.
13 C. G. Elles, A. E. Jailaubekov, R. A. Crowell and S. E. Bradforth, Excitation-Energy Dependence of the Mechanism for Two-Photon Ionization of Liquid H_2O and D_2O from 8.3 to 12.4 eV, *J. Chem. Phys.*, 2006, **125**, 044515.
14 C. G. Elles, I. A. Shkrob, R. A. Crowell and S. E. Bradforth, Excited State Dynamics of Liquid Water: Insight from the Dissociation Reaction Following Two-Photon Excitation, *J. Chem. Phys.*, 2007, **126**, 164503.
15 X. Shi, F. H. Long, H. Lu and K. B. Eisenthal, Electron Solvation in Neat Alcohols, *J. Phys. Chem.*, 1995, **99**, 6917–6922.
16 T. Scheidt and R. Laenen, Ionization of Methanol: Monitoring the Trapping of Electrons on the fs Time Scale, *Chem. Phys. Lett.*, 2003, **371**, 445–450.
17 B. Soroushian, I. Lampre, P. Pernot, V. De Waele, S. Pommeret and M. Mostafavi, Formation and Geminate Recombination of Solvated Electron upon Two-Photon Ionisation of Ethylene Glycol, *Chem. Phys. Lett.*, 2004, **394**, 313–317.
18 A. Thaller, R. Laenen and A. Laubereau, The Precursors of the Solvated Electron in Methanol Studied by Femtosecond Pump-Repump-Probe Spectroscopy, *J. Chem. Phys.*, 2006, **124**, 024515.
19 J. Urbanek, A. Dahmen, J. Torres-Alacan, P. Königshoven, J. Lindner and P. Vöhringer, Femtosecond Two-Photon Ionization and Solvated Electron Geminate Recombination in Liquid-to-Supercritical Ammonia, *J. Phys. Chem. B*, 2012, **116**, 2223–2233.
20 J. Urbanek and P. Vöhringer, Vertical Photoionization of Liquid-to-Supercritical Ammonia: Thermal Effects on the Valence-to-Conduction Band Gap, *J. Phys. Chem. B*, 2013, **117**, 8844–8854.
21 J. A. Kloepfer, V. H. Vilchiz, V. A. Lenchenkov and S. E. Bradforth, Femtosecond Dynamics of Photodetachment of the Iodide Anion in Solution: Resonant Excitation into the Charge-Transfer-to-Solvent State, *Chem. Phys. Lett.*, 1998, **298**, 120–128.
22 H. Iglev, M. K. Fisher and A. Laubereau, Electron Detachment from Anions in Aqueous Solutions Studied by Two- and Three-Pulse Femtosecond Spectroscopy, *Pure Appl. Chem.*, 2010, **82**, 1919–1926.
23 A. E. Bragg and B. J. Schwartz, The Ultrafast Charge-Transfer-to-Solvent Dynamics of Iodide in Tetrahydrofuran. 1. Exploring the Roles of Solvent and Solute Electronic Structure in Condensed-Phase Charge-Transfer Reactions, *J. Phys. Chem. B*, 2008, **112**, 483–494.
24 A. E. Bragg and B. J. Schwartz, Ultrafast Charge-Transfer-to-Solvent Dynamics of Iodide in Tetrahydrofuran. 2. Photo-induced Electron Transfer to Counterions in Solution, *J. Phys. Chem. A*, 2008, **112**, 3530–3543.
25 F. Messina, O. Bräm, A. Cannizzo and M. Chergui, Real-Time Observation of the Charge Transfer to Sovent Dynamics, *Nat. Commun.*, 2013, **4**, 2119, DOI: 10.1038/ncomms3119.
26 A. Kothe, M. Wilke, A. Moguilevski, N. Engel, B. Winter, I. Y. Kiyan and E. F. Aziz, Charge Transfer to Solvent Dynamics in Iodide Aqueous Solution Studied at Ionization Threshold, *Phys. Chem. Chem. Phys.*, 2015, **17**, 1918–1924.
27 M. J. Blandamer and M. F. Fox, Theory and Applications of Charge-Transfer-To-Solvent Spectra, *Chem. Rev.*, 1970, **70**, 59–93.

28 E. R. Barthel, I. B. Martini and B. J. Schwartz, Direct Observation of Charge-Transfer-To-Solvent (CTTS) Reactions: Ultrafast Dynamics of the Photoexcited Alkali Metal Anion Sodide (Na^-), *J. Chem. Phys.*, 2000, **112**, 9433–9444.
29 J. A. Kloepfer, V. H. Vilchiz, V. A. Lenchenkov, A. C. Germaine and S. E. Bradforth, The Ejection Distribution of Solvated Electrons Generated by the One-Photon Photodetachment of Aqueous I^- and Two-Photon Ionization of the Solvent, *J. Chem. Phys.*, 2000, **113**, 6288–6307.
30 W.-S. Sheu and P. J. Rossky, Electronic and Solvent Relaxation Dynamics of a Photoexcited Aqueous Halide, *J. Chem. Phys.*, 1996, **100**, 1295–1302.
31 A. Staib and D. Borgis, Reaction Pathways in the Photodetachment of an Electron from Aqueous Chloride: A Quantum Molecular Dynamics Study, *J. Chem. Phys.*, 1996, **104**, 9027–9039.
32 P. Vörhinger, Ultrafast Dynamics of Electrons in Ammonia, *Annu. Rev. Phys. Chem.*, 2015, **66**, 97–118.
33 Á. Carrera and E. Marceca, Electric Deflection of Middle-Size Ammonia Clusters Containing (e^-, Na^+) Pairs, *J. Phys. Chem. A*, 2015, **119**, 4207–4213.
34 G. Sciaini, E. Marceca and R. Fernández-Prini, Development of the Charge-Transfer-To-Solvent Process with Increasing Solvent Fluid Density: The Effect of Ion Pairing, *Phys. Chem. Chem. Phys.*, 2006, **8**, 4839–4848.
35 G. Sciaini, E. Marceca and R. Fernández-Prini, Influence of Ion Pairing on the UV-Spectral Behavior of KI Dissolved in Supercritical NH_3: From Vapor Phase to Condensed Liquid., *J. Phys. Chem. B*, 2005, **109**, 18949–18955.
36 C. A. Werley, S. M. Teo and K. A. Nelson, Pulsed laser noise analysis and pump-probe signal detection with a data acquisition card, *Rev. Sci. Instrum.*, 2011, **82**, 123108.
37 L. Haar and J. S. Gallagher, Thermodynamic Properties of Ammonia, *J. Phys. Chem. Ref. Data*, 1978, **7**, 635–792.
38 W. C. Johnson and R. I. Martens, The Density of Solutions of Alkali Metal Halides in Liquid Ammonia, *J. Am. Chem. Soc.*, 1936, **58**, 15–18.
39 H. Iglev, A. Trifonov, A. Thaller, I. Buchvarov, T. Fiebig and A. Laubereau, Photoionization Dynamics of an Aqueous Iodide Solution: The Temperature Dependence, *Chem. Phys. Lett.*, 2005, **403**, 198–204.
40 J. Urbanek and P. Vöhringer, Below-Band-Gap Ionization of Liquid-to-Supercritical Ammonia: Geminate Recombination via Proton-Coupled Back Electron Transfer, *J. Phys. Chem. B*, 2014, **118**, 265–277.
41 E. Grunwald, Interpretation of Data Obtained in Nonaqueous Media, *Anal. Chem.*, 1954, **26**, 1696–1701.
42 S. Winstein, E. Clippinger, A. H. Fainberg and G. C. Robinson, Salt Effects and Ion-Pairs in Solvolysis, *J. Am. Chem. Soc.*, 1954, **76**, 2597–2598.
43 H. Sadek and R. M. Fuoss, Electrolyte-Solvent Interaction. V. Tetrabutylammonium Bromide in Ethanol-Carbon Tetrachloride Mixtures, *J. Am. Chem. Soc.*, 1954, **76**, 5902–5904.
44 M. Eigen and K. Tamm, Schallabsorption in Elektrolytlösungen als Folge Chemischer Relaxation. I. Relaxationstheorie der Mehrstufingen Dissoziation, *Z. Elektrochem.*, 1962, **66**, 93–107.
45 V. F. Hnidza and C. A. Kraus, Properties of Electrolytic Solutions. XXXIX. Conductance of Several Salts in Ammonia at -34° by a Precision Method, *J. Am. Chem. Soc.*, 1949, **71**, 1565–1575.
46 R. A. Robinson and R. H. Stokes, *Electrolyte Solutions*, Dover Publications Inc., Mineola, New York, 2nd revised edn, 2002, pp. 392–397.
47 M. Buback and W. D. Harder, The Static Dielectric Constant of Ammonia to High Pressures and Temperatures II. Representation of Experimental Data *via* Kirkwood-Fröhlich's Equation, *Ber. Bunsen-Ges.*, 1977, **81**, 609–614.
48 D. Shapira and A. Treinin, Charge-Transfer-to-Solvent Spectra in Liquid Ammonia, *J. Phys. Chem.*, 1966, **70**, 305–306.
49 J. A. Kloepfer, V. H. Vilchiz, V. A. Lenchenkov, X. Chen and S. E. Bradforth, Time-Resolved Scavenging and Recombination Dynamics from $I{:}e^-$ Caged Pairs, *J. Chem. Phys.*, 2002, **117**, 766–778.
50 P. Krebs, Localization of Excess Electrons in Dense Polar Vapours, *J. Phys. Chem.*, 1984, **88**, 3702–3709.
51 K. A. Tay, F.-X. Coudert and A. Boutin., Mechanism and Kinetics of Hydrated Electron Diffusion, *J. Chem. Phys.*, 2008, **129**, 054505.
52 Y. Harima and S. Aoyagui, The Diffusion Coefficient of Solvated Electrons in Liquid Ammonia, *J. Electroanal. Chem.*, 1980, **109**, 167–177.
53 J. Lindner, A.-N. Unterreiner and P. Vöhringer, Femtosecond Relaxation Dynamics of Solvated Electrons in Liquid Ammonia, *ChemPhysChem*, 2006, **7**, 363–369.
54 V. H. Vilchiz, J. A. Kloepfer, A. C. Germaine, V. A. Lenchenkov and S. E. Bradforth, Map for the Relaxation Dynamics of Hot Photoelectrons Injected into Liquid Water *via* Anion Threshold Photodetachment and above Threshold Solvent Ionization, *J. Phys. Chem. A*, 2001, **105**, 1711–1723.
55 L. M. Dorfman and B. Bockrath, Pulse Radiolysis Studies. XXII. Spectrum and Kinetics of the Sodium Cation-Electron Pair in Tetrahydrofuran Solutions, *J. Phys. Chem.*, 1973, **77**, 1002–1006.
56 L. M. Dorfman and F. Y. Jou, Pulse Radiolysis Studies. XXI. Optical Absorption Spectrum of the Solvated Electron in Ethers and in Binary Solutions of these Ethers, *J. Chem. Phys.*, 1973, **58**, 4715–4723.